31 Kohn-Sham Master Equation Approach to Transport Through Single Molecules

R. Gebauer, K. Burke, and R. Car

31.1 Introduction

In recent years it has become possible to study experimentally charge transport through single molecules [Nitzan 2003]. Typically, the devices in which such experiments can be realized consist of metal-molecule-metal junctions, where two metallic leads are connected by some molecule. Such junctions are expected to be at the basis of future molecular-based electronic devices. But apart from technological applications, these experiments can also be taken as a basis for understanding electron tunneling in general.

The theoretical modeling of molecular transport, however, is a very challenging task: On one hand, it is intuitively clear that the conduction properties of a molecular junction will crucially depend on details of the chemical bonding, particularly at the interface between the metal electrodes and the molecule. Such properties are routinely studied using methods based on density-functional theory (DFT) [Hohenberg 1964]. On the other hand, ground-state theories like DFT cannot be directly applied to systems with a finite current, because such devices are out of equilibrium.

A standard methodology that allows to calculate transport properties from first principles is based on non-equilibrium Green's functions (NEGF) [Keldysh 1965]. In this framework, which is today adopted for almost all calculations in this field, the current is obtained by solving an elastic scattering problem with open boundaries through which electrons are injected from the leads. The NEGF formalism is often used together with DFT in order to achieve chemical accuracy also in systems containing several tens to hundreds of atoms. The NEGF method is explained in detail in Chap. 32 of this book.

Here we present an alternative formulation that can be seen as a generalization of the Boltzmann transport equation (BTE) [Ashcroft 1976] to the fully quantum mechanical case. The BTE is a very successful approach to study transport in non-equilibrium systems. In contrast to NEGF formalisms, where energy-dependent scattering problems are solved, the BTE is formulated in the time-domain: Electrons are accelerated by an external driving force (an electric field, for instance), and the energy which is injected in this way into the system is dissipated by inelastic scattering events. The interplay between acceleration and dissipation leads to a *steady state* in which

R. Gebauer et al.: *Kohn-Sham Master Equation Approach to Transport Through Single Molecules*, Lect. Notes Phys. **706**, 463–477 (2006)
DOI 10.1007/3-540-35426-3_31

a finite, time-independent current flows through the system. The BTE is a semi-classical theory that is formulated in terms of *wave packets* whose dimensions in space are typically of the order of several tens of nanometers. It is therefore clear that the BTE cannot be used to study molecular junctions where chemical details on the atomistic scale need to be taken correctly into account.

In this chapter we show how it is possible to generalize the Boltzmann approach to quantum systems at the nanoscale, and how transport can be treated as a time-dependent problem in this framework.

31.2 Modeling a Molecular Junction

The first step towards a computational treatment of electron transport through single molecules is the choice of a suitable model geometry in which the calculations are performed. Experimentally the nanojunctions are placed between two metallic contacts. Such contacts can be for example the tip of a scanning tunneling microscope (STM), or a metallic surface on which a molecular layer is assembled. Those metallic contacts are then connected via the leads to an external power source, e.g., to a battery. In standard NEGF calculations, this setup is modeled using *open boundary conditions* in the contacts, and the leads outside the computational box on both sides of the molecule are considered semi-infinite, as shown in the upper panel of Fig. 31.1.

31.2.1 Periodic Boundary Conditions

In contrast to the usual approach, we model the molecular junction using a so-called *ring geometry*: the molecule together with a finite piece of the metallic contacts is repeated periodically. This setup, which represents a closed circuit in which no electrons can be exchanged with the exterior, is shown in the middle and lower panel of Fig. 31.1.

In order to induce an electrical current in this ring, one needs to apply an external electromotive force. In our calculations we use a spatially constant electric field $\boldsymbol{\mathcal{E}}$ to accelerate the electrons. Often such a field is represented using a scalar potential $v_{\boldsymbol{\mathcal{E}}}(\boldsymbol{r}) = -\boldsymbol{\mathcal{E}} \cdot \boldsymbol{r}$. This choice, called *position gauge*, is however impossible in a ring geometry with periodic boundary conditions, because the $\boldsymbol{r}$-operator is not periodic and not bounded from below. Instead, we represent $\boldsymbol{\mathcal{E}}$ using a time-dependent vector potential $\boldsymbol{A}(t) = -c\boldsymbol{\mathcal{E}}t$ that is, like the electric field, uniform in space and therefore compatible with periodic boundary consitions. The price to pay for the use of this so-called *velocity gauge* is that the Hamiltonian now becomes explicitly time-dependent. In our framework this is not a problem, because we aim at a kinetic approach in the spirit of the BTE, in which the quantum system is propagated in time until it reaches a steady state.

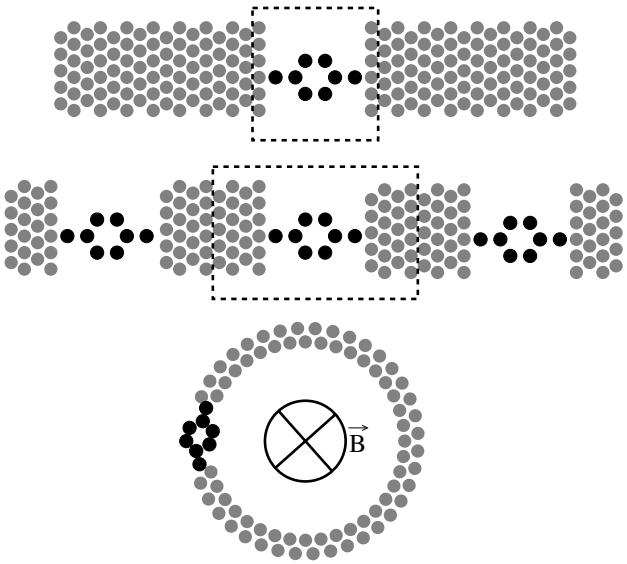

Fig. 31.1. *Upper panel*: Molecular junction with semi-infinite leads and open boundary conditions. *Middle panel*: Periodic geometry where the molecule and a piece of metal is repeated periodically. This can also be imagined as a ring geometry (*lower panel*). The electric field in the ring is induced by a magnetic flux inside the ring. The dashed boxes represent the computational cells with open and closed boundary conditions, respectively

One way to visualize the origin of the vector potential $\boldsymbol{A}(t)$ is by imagining a magnetic field in the center of the ring (but outside the material itself), as schematically shown in Fig. 31.1. If that field increases with time, then an electric field is induced that accelerates the electrons in the ring.

One obvious problem arising from this choice of gauge is that $\boldsymbol{A}(t)$ is not bounded, and as the vector potential increases indefinitely, the Hamiltonian becomes singular. We avoid this by performing gauge transformations in regular intervals, as explained in Sect. 31.4.

31.2.2 The Role of Dissipation

The external electric field that is applied to the ring accelerates the electrons. In a system through which a finite current is flowing, this means that energy is injected and that the electrons are driven away from equilibrium. They will however not settle in a steady state with constant current flowing through the junction, but continue to be accelerated and gain more and more energy. This situation does not correspond to the physics we want to model: In the experimental setup a finite voltage applied to the molecule generally results in a constant current flowing through the junction.

The missing element in our model is therefore a way to *dissipate energy*. In the BTE dissipation is described using a *collision term* that accounts for the scattering of wavepackets with phonons, impurities or other electrons. In the case of transport through a molecule, the situation is slightly different than in this semiclassical case. The small size of the molecules allows for a quasi ballistic transport on the lengthscale of the junction. It is therefore often a good approximation to neglect scattering in the junction itself.

The situation is different for the metallic contacts. These regions of the device are of mesoscopic, or even macroscopic, size. Here dissipation, mainly by phonons, can generally not be neglected, and as we have seen above this dissipation is crucial to establish a steady state with a finite and constant current. In open boundary methods like the NEGF approach, all these effects far away from the molecule are treated implicitly. One introduces two different quasi-Fermi levels to the left and the right side of the junction, and these effectively contain all the scattering and thermalization processes happening in the large contacts.

In our model we contain only a part of the metallic leads in the simulation cell, and this small metal region must account for all the dissipative effects needed to reach steady state. Since practical computations limit the size of the simulation cell, one can treat in practice only metal regions much smaller than the electronic mean free paths that would be required for thermalization. Computationally, one applies therefore a much stronger dissipation inside small metal contacts than what would be given by a realistic electron-phonon coupling strength. In this way, one can achieve thermalization and steady state with relatively small computational cells.

31.3 Master Equations

As discussed above, dissipation is a crucial ingredient for our quantum kinetic approach. One can consider that the system (the electrons in our case) is in contact with a *heat bath* (the phonons), that allows energy transfer between the system and its environment and tends to bring the system towards thermal equilibrium at a given bath temperature T. From that point of view it is clear that the electrons cannot be described simply by wavefunctions: At finite T the equilibrium is given by a statistical average of electronic eigenstates with different energies. Such statistical averages are commonly described using *density matrices*. Let $\hat{\rho}$ be the density matrix of our electronic system, then we have in equilibrium

$$\hat{\rho}^{\mathrm{eq}} = \sum_i n_i^0 \, |i\rangle\langle i| \ , \tag{31.1}$$

where $|i\rangle$ are the eigenstates of the system and n_i^0 are thermal occupation numbers.

31.3.1 Master Equation

If an external bias is applied to the electrons, then $\hat{\rho}$ is driven away from $\hat{\rho}^{\mathrm{eq}}$. The dynamics followed by the density matrix is given by the *master equation*, which in our case has the form

$$\frac{\mathrm{d}}{\mathrm{d}t}\hat{\bar{\rho}}(t) = -\mathrm{i}\left[\hat{H}(t), \hat{\bar{\rho}}(t)\right] + \breve{\mathcal{C}}\left[\hat{\bar{\rho}}(t)\right] . \tag{31.2}$$

Here, $\hat{H}(t)$ contains the external electric field, and the collision term $\breve{\mathcal{C}}[\cdots]$ describes the inelastic scattering with the heat bath. Equation (31.2) with only the first term on the r.h.s. corresponds simply to the time-dependent Schrödinger equation, written for density matrices rather than wavefunctions.

The collision term, which tends to bring the system to its thermal equilibrium, induces transitions between eigenstates of the system. An electron that is placed initially in an excited eigenstate remains there forever if no interaction with the bath is present. With the term $\breve{\mathcal{C}}[\hat{\bar{\rho}}]$ however, there will be a finite probability for the electron to lose energy and go towards a lower unoccupied eigenstate. These transitions between eigenstates are incorporated using Fermi's golden rule that determines which transitions are energetically allowed in presence of a phonon with a given frequency. Because Fermi's golden rule relies implicitly on an averaging procedure in time (all energetically forbidden transitions are oscillatory and average therefore to zero), also the action of $\breve{\mathcal{C}}[\cdots]$ implies such an averaging. We indicate this fact using a *bar* for the averaged $\hat{\bar{\rho}}(t)$ in (31.2).

The derivation of an explicit form for the collision term relies on two major approximations. The first is to assume that the interaction between the electrons and the bath is *weak* and that one can therefore apply perturbation theory. This approximation is usually a very good one, the electron-phonon interaction, for example, can indeed be very well described using a perturbative approach. The second approximation, which is often much more delicate, is the so-called Markov approximation. One assumes that the heat bath is always in thermal equilibrium and that all interactions with the bath are instantaneous processes. In this way the dynamics of the system at time t is only given by its state $\hat{\rho}(t)$ at the same time, and not by its history. This approximation is of course closely related to the use of time-averaging in $\breve{\mathcal{C}}[\hat{\bar{\rho}}(t)]$ and the application of Fermi's golden rule, as discussed above.

Using these approximations, an explicit form of the collision term is derived in many textbooks [Louisell 1973, Cohen-Tannoudji 1992]. Here we only state the result, which can be cast in the form

$$\breve{\mathcal{C}}\left[\hat{\bar{\rho}}(t)\right] = -\sum_{l,m} \gamma_{lm} \left\{ \hat{L}_{ml}\hat{L}_{lm}\hat{\bar{\rho}}(t) + \hat{\bar{\rho}}(t)\hat{L}_{ml}\hat{L}_{lm} - 2\hat{L}_{lm}\hat{\bar{\rho}}(t)\hat{L}_{ml} \right\} . \tag{31.3}$$

Here the $\hat{L}_{ij}$ are operators representing an electronic transition from eigenstate $|j\rangle$ to $|i\rangle$: $\hat{L}_{ij} = |i\rangle\langle j|$. The numbers γ_{ij} define the strength of

the coupling to the bath for each possible electronic transition. They are given by

$$\gamma_{ij} = \begin{cases} \left|\langle i|\hat{V}_{\mathrm{e-ph}}|j\rangle\right|^2 \left[\bar{n}(\varepsilon_j - \varepsilon_i) + 1\right] & \varepsilon_i < \varepsilon_j \\ \left|\langle i|\hat{V}_{\mathrm{e-ph}}|j\rangle\right|^2 \left[\bar{n}(\varepsilon_i - \varepsilon_j)\right] & \varepsilon_i > \varepsilon_j \end{cases} . \tag{31.4}$$

$V_{\mathrm{e-ph}}$ is the electron-phonon interaction potential, ε_i, ε_j are the energies of the electronic eigenstates $|i\rangle$ and $|j\rangle$, respectively, and $\bar{n}(\omega)$ is the thermal mean occupation number of phonons with energy ω: $\bar{n}(\omega) = 1/(\mathrm{e}^{\omega/kT} - 1)$. It is important to note that in (31.4) the probability of an electronic transition downwards in energy is higher than the probability for a jump upwards. This symmetry breaking is a true quantum effect: Induced emission and absorption of phonons have the same probability, but an electron can also jump to a lower energy level by spontaneous emission of a phonon. These spontaneous emission processes are the origin of the breaking of symmetry, and allow the system to reach thermal equilibrium.

As already mentioned in Sect. 31.2.2, we limit our $\hat{V}_{\mathrm{e-ph}}$ to the metal region of the ring. Moreover, we increase the coupling constants γ_{ij} by an overall factor γ_0 that can vary from roughly 100 to 1000. This allows us to reach a steady state using a relatively small metallic region.

31.3.2 TDDFT and a KS Master Equation

In order to carry out realistic calculations, the scheme set up in the previous sections needs to be made computationally tractable. The computational cell typically contains hundreds to thousands of electrons, and it is of course impossible to work in terms of the exact many-particle wavefunctions or density matrices.

It is possible to describe the dissipative many-electron system, evolving under the master equation (31.2) using a generalization of DFT to dissipative systems [Burke 2005b]. In the same way as in standard DFT one can prove that the potential is uniquely determined (up to an arbitrary additional constant) by the charge density $n(\boldsymbol{r})$, it is possible to show that for a dissipative quantum system no two different one-body potentials can give rise to the same time-dependent density $n(\boldsymbol{r}, t)$, given the superoperator $\check{\mathcal{C}}$ in (31.2) and an initial density matrix $\hat{\rho}(0)$. This theorem establishes a DFT for quantum systems evolving under a master equation. For the use in practical calculations one constructs a corresponding KS system. In that system of non-interacting electrons, the one-body potential $v_{\mathrm{KS}}[n, \hat{\rho}_{\mathrm{KS}}(0), \check{\mathcal{C}}]$ is defined such that it yields the exact density $n(\boldsymbol{r}, t)$ of the interacting system.

Defined in this way, the KS system has certain pathologies. The superoperator in the many-body master equation is guaranteed to vanish only on the many-body equilibrium density matrix, but not necessarily on the equlibrium KS density matrix. To avoid this problem, we modify the master equation

by introducing a KS form of the superoperator $\breve{\mathcal{C}}$ in terms of the *single particle reduced density matrix* $\hat{\rho}_{\mathrm{KS}}(t)$. To this end, we define the single-particle potential $v_{\mathrm{KS}}(T)(\boldsymbol{r})$ as the KS potential in the Mermin functional at temperature T, i.e., the potential that, when thermally occupied with non-interacting electrons, reproduces the exact density at thermal equilibrium. The KS states $|\alpha\rangle$ defined in this way (which we designate with Greek letters to distinguish them from the many particle eigenstates $|i\rangle$ above) are used as a basis for the density matrix:

$$\hat{\tilde{\rho}}_{\mathrm{KS}}(t) = \sum_{\alpha,\beta} f_{\alpha\beta}(t)|\alpha\rangle\langle\beta| \,. \tag{31.5}$$

To find the KS master equation itself, we reduce the many-body (31.2) to a single-particle form by tracing out all other degrees of freedom, and use a Hartree-style approximation for the two-particle correlation functions appearing in the collision term. In this way we find for the coefficients $f_{\alpha\beta}$ in (31.5):

$$\begin{aligned}\frac{\mathrm{d}}{\mathrm{d}t} f_{\alpha\beta} = -\mathrm{i} \sum_{\lambda} \left(H_{\alpha\lambda} f_{\lambda\beta} - f_{\alpha\lambda} H_{\lambda\beta}\right) + \left(\delta_{\alpha\beta} - f_{\alpha\beta}\right) \sum_{\lambda} \frac{1}{2} \left(\gamma_{\alpha\lambda} + \gamma_{\beta\lambda}\right) f_{\lambda\lambda} \\ - f_{\alpha\beta} \sum_{\lambda} \frac{1}{2} \left(\gamma_{\lambda\alpha} + \gamma_{\lambda\beta}\right) \left(1 - f_{\lambda\lambda}\right) \,. \end{aligned} \tag{31.6}$$

Equation (31.6) is the final form for the master equation used in our calculations. It can be viewed as a generalization of the BTE to the full quantum case, as it is formulated in terms of the density matrix rather than in terms of wavepackets. The first term in the r.h.s. represents the Hamiltonian propagation. The $H_{\alpha\beta}$ are the matrix elements of the time-dependent KS Hamiltonian in the basis of the unperturbed orbitals. The second and third terms in the r.h.s. represent the collision terms. One can verify that (31.6) satisfies a series of important properties for a master equation: The trace of $\hat{\rho}$ is invariant, guaranteeing a constant number of electrons in the system. Furthermore, $\hat{\rho}$ stays Hermitian during the time propagation and, in the absence of external perturbations, tends to the Fermi-Dirac distribution as its thermal equilibrium state. Finally, one can show that the collision terms act to reduce the off-diagonal elements $f_{\alpha\beta}$ while pushing the system towards equilibrium.

31.4 Practical Aspects

31.4.1 Time Propagation

The complete single particle density matrix $\hat{\rho}$ has the dimension $(N_{\mathrm{occ}} + N_{\mathrm{unoc}}) \times (N_{\mathrm{occ}} + N_{\mathrm{unocc}}) = M \times M$, where M is the size of the basis set and N_{occ}, N_{unocc} are the number of occupied and unoccupied KS states,

respectively. In practice, it is often impossible to treat the full $M \times M$ matrix in the master equation (31.6). In such cases, the computational load can be significantly reduced by explicitly including only the basis states $|\alpha\rangle$ within a given energy window around the Fermi energy. All states with an energy below this range are considered occupied, all higher lying states are neglected. In this way the time propagation can be carried out even in systems where a large basis set (like, e.g., plane waves) is used to describe the ground state electronic structure.

In practice, the time integration in (31.6) is carried out in the following way: From a given time t the density matrix is propagated for a finite period $\tau_{\mathcal{E}}$ using only the Hamiltonian propagator with the time-dependent vector potential, corresponding to the first term in the r.h.s. of (31.6). Let us choose the x-direction along the circumference of the ring, and assume that the unit cell is of size L in this direction. The electric field $\boldsymbol{\mathcal{E}} = \mathcal{E}\mathbf{e}_x$ is then also directed along $\mathbf{e}_x$, and we can choose $\tau_{\mathcal{E}} = 2\pi/(\mathcal{E}L)$. In this case, the vector potential changes in that period from $\boldsymbol{A}(t)$ to $\boldsymbol{A}(t) - 2\pi c\mathbf{e}_x/L$. At this point, is is possible to perform a *gauge transformation* by adding to the vector potential $2\pi c\mathbf{e}_x/L$ and at the same time multiplying all electronic wavefunctions with a phase factor $\exp(-\mathrm{i}2\pi x/L)$. These phase factors are compatible with periodic boundary conditions. In this way one avoids a vector potential that increases indefinitely. After the Hamiltonian time propagation plus gauge transformation, the density matrix is propagated for the same time interval $\tau_{\mathcal{E}}$ using the collision term only, corresponding to the second and third terms in the r.h.s. of (31.6). After this procedure one obtains the density matrix $\bar{\rho}(t + \tau_{\mathcal{E}})$. In the limit $L \to \infty$, the time $\tau_{\mathcal{E}}$ tends to zero, and this integration procedure converges to the exact solution of the master equation.

31.4.2 Calculating Currents

One important quantity to calculate in this kinetic scheme is of course the current, as it is the central quantity characterizing transport through the molecule. The current $\boldsymbol{j}(\boldsymbol{r}, t)$ must satisfy the current continuity equation

$$\frac{\mathrm{d}}{\mathrm{d}t} n(\boldsymbol{r}, t) + \nabla \cdot \boldsymbol{j}(\boldsymbol{r}, t) = 0\,, \tag{31.7}$$

which translates the fact that charges are locally conserved [$n(\boldsymbol{r}, t)$ is the charge density]. It is well known that the Hamiltonian propagation does satisfy (31.7), if the current is defined as

$$\boldsymbol{j}_H(\boldsymbol{r}, t) = \mathrm{Tr}\left[\hat{\bar{\rho}}(t)\hat{\boldsymbol{J}}(\boldsymbol{r})\right], \tag{31.8a}$$

$$\hat{\boldsymbol{J}}(\boldsymbol{r}) \quad = \frac{1}{2}\left\{[\hat{\boldsymbol{p}} + \boldsymbol{A}(t)/c]\,\delta(\boldsymbol{r} - \hat{\boldsymbol{r}}) + \delta(\boldsymbol{r} - \hat{\boldsymbol{r}})\,[\hat{\boldsymbol{p}} + \boldsymbol{A}(t)/c]\right\}. \tag{31.8b}$$

In the case of our master dynamics however, the current $\boldsymbol{j}_H$ defined in this way does not satisfy the continuity equation. The reason for this is again

the time-averaging procedure that underlies the collision term $\breve{\mathcal{C}}[\hat{\rho}]$ that we mentioned above in Sect. 31.3. As explained there, the use of Fermi's golden rule in our scheme implies performing time integrals over many oscillations of electronic transitions. Mapping this time-dependent process on an instantaneous scattering event amounts to neglecting all electronic currents that flow during that time, and, as a consequence, the continuity equation is not satisfied.

It is possible to recover the missing term of the current that originates from the interaction with the bath. This term, which we call *collision* or *dissipative* current $\boldsymbol{j}_{\mathcal{C}}(\boldsymbol{r},t)$ restores the local charge conservation, and the total *physical* current (which is measuread in experiments) is the sum $\boldsymbol{j}(\boldsymbol{r},t) = \boldsymbol{j}_H(\boldsymbol{r},t) + \boldsymbol{j}_{\mathcal{C}}(\boldsymbol{r},t)$. An explicit form for the dissipative current is given elsewhere [Gebauer 2004a].

31.5 Results

This quantum kinetic scheme has been used for both realistic and model calculations, which we will briefly outline in the following.

31.5.1 Model Calculation

To illustrate our methodology, we consider in the following a one-dimensional test system consisting of a double-barrier resonant tunneling structure (DBRTS) [Gebauer 2004b]. We treat electron-electron interactions on the Hartree level, allowing therefore to study the key elements of this scheme only, without discussing more sophisticated exchange and correlation effects.

The external $v_{\text{ext}}(x)$ in absence of an applied electric field is shown in the upper panel on the left of Fig. 31.2. The double barrier constitutes the junction and is set into a periodically repeated unit cell as shown in the figure. Outside the barrier region, we assume a carrier density of $4.3\times10^{18}\,\text{cm}^{-3}$, and choose an effective mass of $0.1\,\text{m}_\text{e}$ and a dielectric constant of 10. The phonon density of states $\mathcal{D}(\omega) \propto \omega^2$, and the electron-phonon couplings $\gamma_{\alpha\beta} = \gamma_0$ for all states α, β. We choose values of 0.136 meV and of 0.218 meV, respectively, for γ_0, and a temperature of 25.3 K, so that k_BT is comparable to the electronic level spacing at the Fermi energy in our finite system ($L = 244\,\text{nm}$). We solve (31.6) for steady state behavior, i.e. $\mathrm{d}f_{\alpha\beta}/\mathrm{d}t = 0$, and determine the Hartree potential self-consistently, for different values of the applied external field $\mathcal{E}$. The total potential acting on the electrons when $\mathcal{E}$ corresponds to peak current is shown in the middle panel on the left of Fig. 31.2. The total potential includes $v_{\text{ext}}(x)$, the externally applied bias [represented by a linearly varying potential $v_{\mathcal{E}}(x) = -\mathcal{E}\cdot x$], and the Hartree potential. We have transformed to the position gauge here only for illustration.

The total potential has the same qualitative behavior found in self-consistent calculations using open boundary conditions for similar model

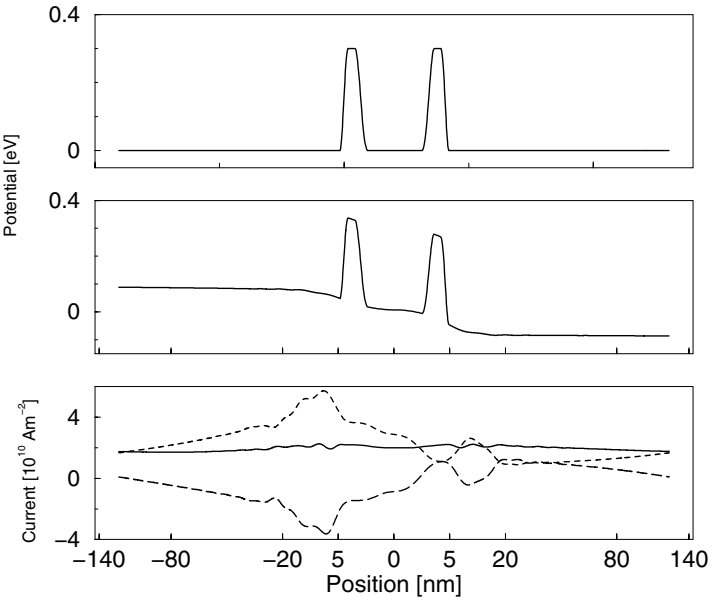

Fig. 31.2. *Upper panel*: the double-barrier resonant tunneling structure in the absence of an electric field. *Middle panel*: total potential at steady state, in presence of an external electric field. *Lower panel*: The currents at steady state. Solid line: total current $j(x)$, long dashed line: collision current $j_{\mathcal{C}}(x)$, short dashed line: Hamiltonian current $j_H(x)$. Please note the non-linear scale of the horizontal axis

systems. In our approach, however, the voltage drop across the barrier is an output of the calculation.

In the lower panel on the left of Fig. 31.2 we plot the expectation values of current densities $j(x)$, $j_{\mathcal{C}}(x)$, and $j_H(x)$ corresponding to the electric field and electron-phonon coupling of the middle panel. In this one-dimensional system at steady state the continuity equation amounts to $\mathrm{d}j(x)/\mathrm{d}x = 0$, the current must therefore be a constant in space. It can be clearly seen in Fig. 31.2 that this is not the case for $j_{\mathcal{C}}$ or j_H separatly, but to a good approximation for the total physical current $j(x)$.

Let us now discuss the current-voltage (I-V) characteristics of this system. From a naïve model in which the bands to the left and right of the barrier are simply shifted rigidly, one obtains the following picture (see also Fig. 31.3): At low bias no current can flow through the system because the electrons see a high barrier blocking any transport (left panel in Fig. 31.3). Only once the bias has reached a threshold value, a localized level between the two barriers enters in resonance with the incoming electrons and allows for a finite current flow (right panel). At very large bias, the localized level falls below lower limit of the occupied bandwidth for the incoming electrons, and current is again suppressed (lower panel).

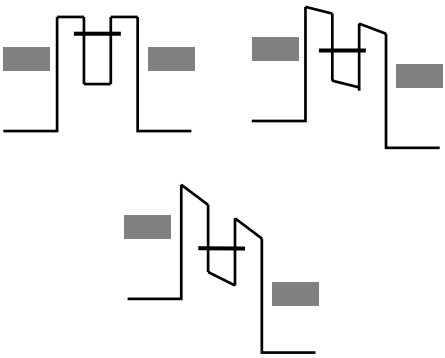

Fig. 31.3. Schematic representation of the transmission behavior of a double-barrier resonant tunneling structure (see text)

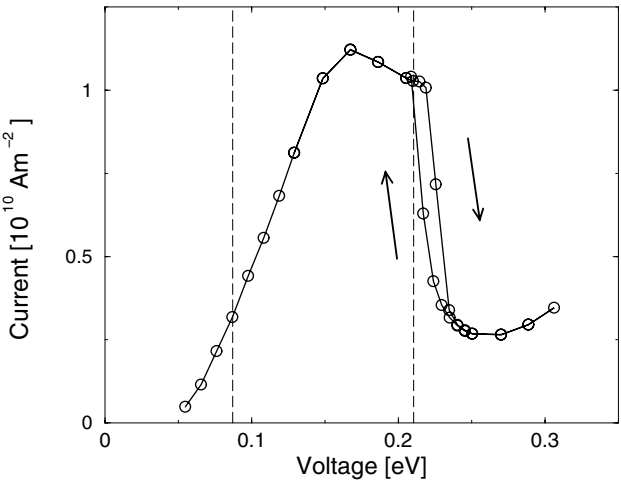

Fig. 31.4. Calculated I-V characteristics of the double-barrier resonant tunneling structure

As shown in Fig. 31.4, our calculated I-V characteristics follow the expected trend. Note that the voltage shown on the horizontal axis is the drop across the barrier structure, rather than the total voltage drop $\mathcal{E} \cdot L$ in the simulation cell. That voltage is an outcome of the self-consistent calculation, rather than an input quantity. The dashed vertical lines indicate the voltages where one would expect current to start respectively stop flowing according to the above considerations.

From this figure we can clearly see that our kinetic model represents correctly the non-linear behavior of the current and intriguing quantum effects like negative differential resistance (NDR) when the current *decreases* with *increasing* applied voltage.

It is interesting to note that the I-V characteristics show a hysteresis loop, depending on whether one goes up or down in the applied electromotive force. This effect is due to the charging of the resonant level at high bias which alters the effective potential barrier seen by the electrons. This hysteresis loop has also been found by other calculations [Jensen 1991, Mizuta 1991].

31.5.2 Realistic Simulations

In the following we report calculations on a molecular electronic device to illustrate further the above concepts. Our circuit consists of a self-assembled monolayer of benzene dithiolate (BDT) molecules in contact with two gold electrodes according to the geometrical setup in Fig. 31.5. Here we briefly mention only a few key computational aspects of these calculations, which are reported elsewhere [Piccinin 2006].

We adopt the adiabatic generalized gradient approximation (GGA) for exchange and correlation and use the PBE [Perdew 1996b] form of the GGA functional. We use norm-conserving pseudopotentials [Troullier 1991] to model the effect of the atomic nuclei plus frozen core electrons on the valence electrons and expand the wavefunctions of the latter in plane waves. Numerically we deal with a discrete set of electronic states calculated at a finite set of k-points in the Brillouin zone of the periodic supercell. With the present choice of k-points the average level spacing at the Fermi energy is around 0.1 eV. As usual in band structure calculations of metallic systems, the discrete distribution of electronic levels is broadened by convoluting it with a Fermi-Dirac distribution (with $k_BT = 0.6\,\text{eV}$ in the present calculation). Given the very small size of our supercell compared to the electronic mean free-path for inelastic phonon scattering, which in gold at room temper-

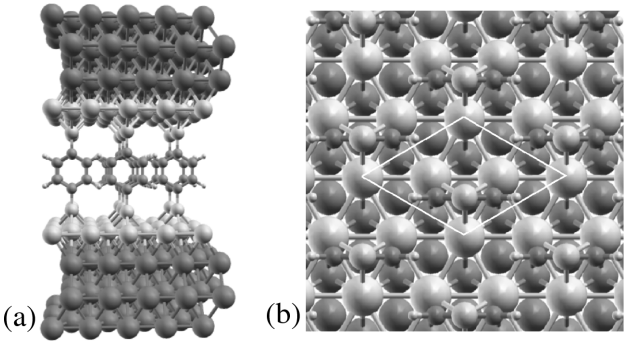

Fig. 31.5. (**a**) Lateral view of the benzene dithiolate (BDT) monolayer between two Au(111) surfaces. A total of 8 layers are included in the unit cell of the simulation. The dark atoms in the slabs indicate the region where dissipation is applied. (**b**) Top view of the BDT monolayer on Au(111): the box indicates the unit cell used in the simulation

ature is of a few hundred Ångström, we use a very crude model for the bath. In particular we neglect inelastic scattering processes in the molecular junction inside the non-shaded region in Fig. 31.5, since electrons traverse this region ballistically to a very good approximation. Inelastic processes needed to thermalize the electrons are confined to the shaded region in Fig. 31.5. To achieve thermalization in such a small space, we adopt an artificially large coupling between the electrons and the bath, similar to what is usually done in non-equilibrium molecular dynamics simulations of classical systems. We also hold the bath at an unphysically large temperature corresponding to the adopted broadening of the energy levels. In spite of these very crude approximations dictated by numerical limitations, the calculation reproduces well a number of the physical features of a real molecular device.

The calculated steady state potential and currents corresponding to an applied electromotive force of 1 eV are reported in Fig. 31.6 [Gebauer 2005]. The potential shows a small linear drop inside the electrodes, as expected

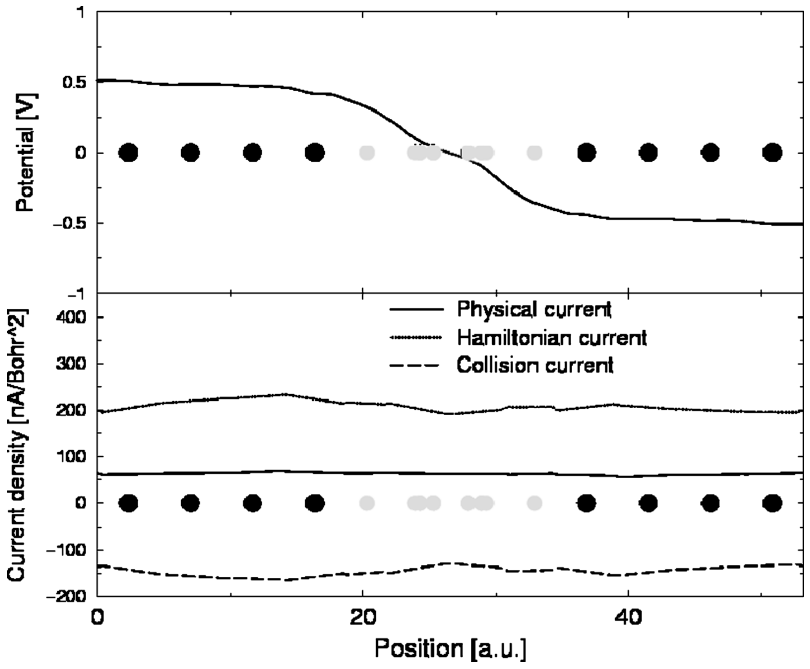

Fig. 31.6. *Top panel*: sum of the externally applied potential and the induced potential at steady state. The externally applied potential is visualized in the position gauge (see text). *Bottom panel*: Hamiltonian current $j_H(r)$, quantum collision current $j_C(r)$ and physical current $j(r) = j_H(r) + j_C(r)$. The electromotive force is applied along the (111) direction, which is shown in the plot. All quantities are averaged over planes perpendicular to the (111) direction. The black dots indicate gold atomic planes. The gray dots indicate BDT atoms

from Ohm's law for a wire of finite resistance when a current circulates. However, most of the potential drop is due to the contact resistance and correctly occurs across the molecular junction. This drop is not purely linear but shows a well defined shoulder within the aromatic ring of the BDT molecules. This reflects the polarization of the ring under the applied bias. The calculated dc current I is about 3.1 μA per DBT molecule, a value that compares well with some recent experiments [Xiao 2004]. Our artificial bath model keeps the distribution of the electrons close to a thermal equilibrium distribution, mimicking real experimental conditions, where the distribution of the electrons injected in a molecular device is close to a thermal equilibrium distribution. Having fixed the strength of the inelastic coupling, the main factor controlling the I-V characteristics of a molecular device like the one in Fig. 31.5 is electron transmission through the molecular junction. Some calculations using an open circuit geometry, which ignore explicit dissipative effects, give a current I which is rather close to the one that we calculate here [Ke 2004]. Notice that the quantum collision current, which originates from inelastic scattering in the shaded regions, is nonzero inside the molecular junction, where it contributes to the observable current density $j(r)$. It should be noticed, however, that the collision current that we calculate here is grossly overestimated due to the artificially large electron-bath coupling required by the small size of our unit cell. Under these circumstances it is better to approximate the physical current with the term (31.8) alone, ignoring the collision current, as the ensuing violations of continuity are usually small [Piccinin 2006].

31.6 Comparison with Standard NEGF Treatment

The standard DFT treatments of single-molecule transport [Di Ventra 2000, Xue 2002] mix ground-state KS density functional theory with the Landauer formalism. This mixture, while intuitive, qualitatively correct for weak correlation, and non-empirical, is not rigorous. By rigorous, we mean it would yield the exact answer if the exact ground-state functional were used. It is clear that the it must fail for, e.g., strong interaction, where Coulomb blockade effects dominate. (Although, see [Toher 2005] for an example that demonstrates that common DFT approximations can produce large overestimates in tunelling currents, within the Landauer formalism.)

Our new formalism *is* rigorous, in the sense that it is based on a DFT theorem that does apply to the present situation. If we knew the exact XC functional for the TDKS Master equation, it would produce the exact answer. The same is true for the work of Chap. 32. Thus, in the limit as $\gamma \to 0$, but keeping γ always finite and the ring large enough to ensure enough scattering occurs in the metal region such that the electrons do not remember their previous encounter with the constriction, the two should yield identical results.

Given the difference in formalisms, it is a major task to compare them to each other, or either to the standard treatment when XC effects are present.

It is much simpler to make the comparison for weak electric fields, where Kubo response theory applies, and dissipative effects can be ignored. Recent work, in the linear response regime, has shown that certain XC electric field effects are missing from the standard treatment [Burke 2005b]. Our dissipative approach recovers the Kubo response in the limit of weak fields [Burke 2005b], and so takes these effects into account.

31.7 Conclusions

In conclusion, we have shown how the semiclassical Boltzmann transport equation can be generalized to treat fully quantum mechanical systems. The resulting master equation allows one to propagate an electronic system in time, under the combined influence of an external driving force and dissipation due to inelastic scattering. We have shown how this general scheme can be applied to the calculation of transport properties, both in model systems and in realistic molecular devices. Further applications of this method to other molecular devices, as well as to electronic conduction through carbon nanotubes, suspended between gold electrodes, are currently in progress.